Iraqi Journal for Computer Science and Mathematics

Volume 6 | Issue 4 Article 2

2025

Retracted: Analysis of Energy Sector CO_2 Emanations Using Wavelet-Based Numerical Technique

Yeshwanth R.
Department of Mathematics, Bangalore University, Bengaluru-560056, yeshuysr@gmail.com

Kumbinarasaiah S.
Department of Mathematics, Bangalore University, Bengaluru-560056, kumbinarasaiah@gmail.com

Recommended Citation

R., Yeshwanth and S., Kumbinarasaiah (2025) "Retracted: Analysis of Energy Sector CO_2 Emanations Using Wavelet-Based Numerical Technique," *Iraqi Journal for Computer Science and Mathematics*: Vol. 6: Iss. 4, Article 2.
DOI: https://doi.org/10.52866/2788-7421.1313
Available at: https://ijcsm.researchcommons.org/ijcsm/vol6/iss4/2

IRAQI JOURNAL FOR COMPUTER SCIENCE AND MATHEMATICS 2026;6:7–20

Retracted: Analysis of Energy Sector CO_2 Emanations Using Wavelet-Based Numerical Technique

Yeshwanth R., Kumbinarasaiah S. *

Department of Mathematics, Bangalore University, Bengaluru-560056

ABSTRACT

This study aims to present the modified Chebyshev wavelet collocation method (CWCM) to investigate and obtain the numerical approximation of CO_2 emissions from the energy sector utilizing the fractional mathematical model. The need for energy rises as the population grows. Burning fossil fuels produces a significant portion of the world's energy, which raises the atmospheric concentration of CO_2 and causes global warming. The combination of mathematical modeling studies and numerical simulations allows us to understand the CO_2 emissions from the energy sector. Our objective is to build an operational matrix of integration (OMI) based on Chebyshev wavelets and use it to the numerical solution of the CO_2 emanation from the energy sector model. Furthermore, these OMI are used to simplify fractional differential equations into an algebraic equation system. Lastly, graphic representations are used to visually present the results and provide empirical support for our theoretical conclusions. Because the CWCM method computes only a few terms and avoids rounding data, it produces correct answers for highly nonlinear situations. We compared the outcomes of the RK4 technique, the ND solver, and the devised method. The numerical results show that CWCM solves the emanation of CO_2 from the energy sector with remarkable accuracy and efficiency in both mathematical and environment view. Software called Mathematica has been used for numerical implementation and calculations.

Keywords: Caputo fractional derivative, Chebyshev wavelet, Collocation method, CO_2 model, Operational matrix of integration
2020 MSC: 34A12, 65L05, 65T60, 34A08.

1. Introduction

Over the past few decades, researchers from various organizations all around the world are investigating mathematical models as practical tools to explain a variety of real-world processes and problems clearly. Mathematical equations can be used to formulate real-world processes, which can then be analyzed for planning, predicting, and other purposes in the future. Mathematical modeling and biology have gained much attention among scholars in recent decades because of the noteworthy [1]. Researchers became interested in fractional calculus because of the drawbacks of the conventional models that described real-world issues using ordinary derivatives or integrals. It is important to note that many aspects of mathematical models cannot yet be adequately explained by ordinary calculus. Therefore, a more thorough explanation of memory and inherited characteristics may be provided by non-integer order derivatives. In this case, a detailed introduction, background information, and critical discoveries were examined, [2] for some significant utilization of those derivatives. The full range of a function is shown by the derivatives of real or complex orders [3]. Furthermore, fractional differential operators provide greater degrees of freedom than integer order. Moreover, [4, 5] for using said region in various real-world issues by numerous scholars. Because many processes and phenomena in the actual world have complicated

Received 28 October 2024; revised 4 January 2025; accepted 9 April 2025.
Available online 25 October 2025

* Corresponding author
E-mail address: kumbinarasaiah@gmail.com (Kumbinarasaiah S.).

https://doi.org/10.52866/2788-7421.1313

geometry and irregular shapes, adequately describing them using standard fractional order derivatives is impossible. Consequently, scholars have developed the idea of fractal derivatives to address these shortcomings of fractional and classical calculus [6, 7]. Here, we point to relevant studies on fractional and fractal operators, where various real-world issues have been examined using fractals-fractional differential (FFD) operators, [8, 9]. The primary advantage of the FFD operator is that it enables the development of models that considerably more precisely represent systems with memory effects.

Here, we look at the CO_2 emissions from the energy sectors inspired by the applications of FFD operators that have been described. An important factor in a country's socioeconomic development is the energy industry. The growing population and expanding economy are driving up energy demand worldwide. Between 2010 and 2040, the world's energy consumption is expected to rise by 56%. [10]. Reports state that burning fossil fuels like coal, gas, and oil accounts for 80% of the world's energy consumption, and that the USA accounted for 76% of all greenhouse gas emissions in the atmosphere in 2017[11]. There is a significant connection between the rise in population and energy use. Therefore, most nations obtain the necessary energy from various sources, such as nuclear reactors or fossil fuels, to ensure the smooth development of their socioeconomic needs. However, the primary reason is the burning of fossil fuels, which directly releases massive amounts of CO_2 into the atmosphere, increasing air pollution and lowering oxygen levels in the surrounding air. The previous factor has recently led to climate change that has caused numerous destructions such as massive floods or earthquakes. Population expansion increases primary energy demand, yet energy accessibility is essential for boosting economic growth and improving living standards. The availability of energy is a critical factor in determining population growth. By improving the amount and quality of energy, energy technology innovation fueled the industrial revolution, which in turn expanded productivity and, ultimately, population. Energy consumption has an impact on the population's carrying capacity as well. The population's carrying capacity and energy consumption rise with new energy sources and technology development [12]. Climate change increases the risk of illnesses connected to food and water contamination, temperature variations, pollution, and other factors directly affecting human health. Reducing energy-related CO2 emissions is crucial to lessening the harmful impacts of global warming.

We refer to [13, 14] for additional relevant studies on the effects of energy resources and CO_2 emissions on the transportation industry. They consider that one of the leading causes of the environment's decreasing CO_2 levels is the growth in the human population. Therefore, a variety of statistical, semi-statistical, and empirical models are used to examine methods for regulating energy use and lowering related CO_2 emissions at the national and regional levels. A thorough grasp of the relationship between mitigation strategies and the reduction of carbon dioxide emissions from the energy sector can be obtained by analytical models that employ qualitative methodologies. Numerous models in mathematics have been studied [15, 16]. It is demonstrated that the suggested model may be constructed using the relationship between the amount of CO_2 in the atmosphere, energy use, and the number of people.

$$\left.\begin{aligned} D_\tau^\beta \mathcal{X}(\tau) &= \lambda + \beta\mathcal{Y} - \delta\mathcal{X} - \psi\mathcal{X}\mathcal{F} \\ D_\tau^\beta \mathcal{Y}(\tau) &= \phi\mathcal{Y}(1-\tfrac{\mathcal{Y}}{L}) - \gamma\mathcal{X}\mathcal{Y} + \mu\eta\mathcal{Y}\mathcal{F} \\ D_\tau^\beta \mathcal{F}(\tau) &= \sigma\mathcal{F}(1-\tfrac{\mathcal{F}}{\mathcal{M}}) - \eta\mathcal{Y}\mathcal{F} + \psi\mu_1\mathcal{X}\mathcal{F} \end{aligned}\right\} \quad (1.1)$$

Tables 1 and 2 describes the dependent variables and parameters of the CO2 model presented in Eq. (1.1).

Small waves or concentrated waves are called wavelets. They fall to zero instead of continuing to oscillate indefinitely. In mathematical study, wavelet theory is a relatively recent development. It has been applied to waveform segmentation and representation in engineering domains such as time-frequency, harmonic, and signal analysis. Wavelets are continuous-time basis functions $\psi_{i,j}(x)$. The wavelet basis is unique because each function $\psi_{i,j}(x)$ is constructed from a single mother wavelet $\psi(x)$, a small pulse that is frequently a collection of linearly independent functions created by translation and dilation of the mother wavelet. Wavelets are a class of functions composed by a single translated and dilated function known as the mother wavelet. Wavelets are based on Joseph Fourier's fundamental idea of superpositioning, which maintains that a complex function can be described by a collection of self-similar components. Wavelet theory has been greatly advanced by the mathematical analysis of Morlet, Stromberg, Meyer, Grossmann, and Daubechies. Even in areas with significant oscillations or gradients, this wavelet-based representation of differential operations can be precise and stable. Its remarkable features, including orthogonality, compact support, and multiresolution analysis, attract many experts. Many dynamical system problems have been solved with approximate solutions based on an orthogonal family of functions. By using truncated orthogonal functions to approximate the distinct

Table 1. Dependent variables with description for emanation of CO_2 from the energy sector.

Dependent variable	Description
$\mathcal{X}$	CO_2 concentration in the atmosphere
$\mathcal{Y}$	Concentration of CO_2 due to human population
$\mathcal{F}$	Concentration of CO_2 due to forest biomass

Table 2. Description and values of the parameters for emanation of CO_2 from the energy sector.

Parameter	Description	Values
λ	Growth rate of atmospheric CO_2 due to natural causes	1
β	Growth rate of CO_2 due to anthropogenic factors	0.05
δ	Natural reduction rate coefficient of atmospheric CO_2	0.003
ψ	Depletion rate of CO_2 due to forest biomass	0.0001
ϕ	Intrinsic growth rate of human population	0.01
$\mathcal{L}$	Carrying capacity of human population	1000
γ	depletion rate coefficient of human population due to CO_2	0.00001
μ	growth of human population due to forest biomass	0.01
η	Deforestation rate coefficient	0.0002
σ	Intrinsic growth rate of forest biomass	0.2
$\mathcal{M}$	Carrying capacity of forest biomass	2000
μ_1	Growth of forest biomass due to CO_2	0.01

signals in the differential equation, one can use orthogonal functions to approximate the underlying differential equation. Another basis set, exceptionally well-localized functions, and wavelets can all be beneficial in solving differential and integral equations. Wavelet methods provide a more accurate, dependable, and exciting way to solve differential and integral equations. Scholars are using wavelet approaches more and more frequently to solve partial and fractional differential equations.

The Chebyshev wavelet is a relatively newer addition to the family of wavelets, rooted in the Chebyshev polynomials, which are known for their optimal properties in approximating functions and minimizing the approximation error. These wavelets combine the properties of Chebyshev polynomials with wavelet theory, making them useful for various signal processing and numerical analysis applications. Chebyshev wavelets are constructed using Chebyshev polynomials of the first kind, which exhibit orthogonality and minimize the maximum error between the polynomial and the target function. The Chebyshev wavelet inherits these properties, allowing for efficient representation and manipulation of functions and signals. The following are Key Properties of Chebyshev Wavelets, **Orthogonality:** Like many wavelet families, Chebyshev wavelets can be made orthogonal, ensuring that the wavelet transform can be inverted without loss of information. Orthogonality simplifies the computation and leads to efficient algorithms for signal processing. **Localization:** Chebyshev wavelets exhibit good localization in both time and frequency domains. This makes them suitable for analyzing non-stationary signals where localized features (such as sharp transitions or edges) are important. **Compact Support:** These wavelets are compactly supported, meaning they are non-zero over a limited range. This is a desirable property for reducing computational complexity, as only a small portion of the signal needs to be processed at each scale and translation. **Minimax Approximation:** One of the distinguishing features of Chebyshev polynomials, and thus Chebyshev wavelets, is their minimax property. This means that they minimize the maximum error when used to approximate a function, which is particularly useful in numerical methods and data compression. **Flexibility in Construction:** Chebyshev wavelets can be constructed for various orders of the Chebyshev polynomial, allowing for a range of smoothness and adaptability depending on the application. Higher-order Chebyshev wavelets provide smoother approximations but at the cost of increased complexity.

Numerous wavelet techniques can be used to solve DE numerically. For instance, U. Lepik et al., [17, 18] investigated the solution of differential equation by the Haar technique. Yeshwanth R. et al. investigated the Chlamydia transmission using the HWM [19], and Darweesh et al. solved Fredholm integro DE using the Haar wavelet method [20]. Manohara et al. employed Bernoulli wavelets on [22] biological models; Shiralashetti S. C. et al. employed Laguerre wavelets [23] to resolve a differential equation system; Preetham et al. addressed Bernoulli wavelet method for the flow of a viscous fluid [24], While Mulimani, developed the solu-

tions of brain tumour model [25], Mishra et al. employed the Taylor wavelet [26] to nonlinear singular value concerns. Yeshwanth R. et al. examined the smoking model [27] using the Haar approach. Kumbinarasaiah S. et al. used the HWM to discuss the impact of global warming [21]. Marriage divorce model through modified Hermite wavelet [28]. The findings obtained are compared to the ND Solver, the CWCM, and the RK4 solution. The recommended plan provides the most straightforward and practical approach to fixing FDEs. Since no one has used CWCM to examine these models in the literature study, we are motivated to investigate this model utilizing the available approaches. This article is organized as follows: Preliminaries are covered in Section 2. Chebyshev wavelet OMI is performed in Section 3. Method of solution and its applications are explained in Sections 4 and 5. The article is concluded in Section 6.

2. Preliminaries of Chebyshev wavelets and fractional derivative

Definition 1: The Caputo fractional derivative of $g(\delta) \in C_\mu$ is defined as [29] :

$$\frac{d^\alpha g(\delta)}{ds^\alpha} = \frac{1}{\Gamma(n-\alpha)} \int_0^\delta (\delta - t)^{n-\alpha-1} g^{(n)}(t) dt$$

For $n-1 < \alpha \leq n$, n is any positive integer, $\delta > 0$, $g(\delta) \in C_\mu^n$, $\mu \geq -1$.

A class of functions called wavelets is made up of the translation and dilation of a single function called the mother wavelet.Allowing the translation parameter (b) and dilation parameter (a) to fluctuate continuously results in a family of continuous wavelets.

$$\psi_{a,b}(\tau) = \sqrt{a}\ \psi\left(\frac{\tau - b}{a}\right), \quad where\ a, b \in \mathbb{R},\ a \neq 0.$$

Definition 2: The family of Chebyshev wavelets are defined in the interval $[0, 1)$ as [30],

$$C_{n,m}(\tau) = \begin{cases} \frac{\alpha_m 2^{\frac{k}{2}}}{\sqrt{\pi}} T_m(2^k\tau - 2n + 1), & \frac{n-1}{2^{k-1}} \leq \tau \leq \frac{n}{2^{k-1}}, \\ 0, & Otherwise, \end{cases}$$

where,

$$\alpha_m = \begin{cases} \sqrt{2}, & m = 0, \\ 2\ , & Otherwise. \end{cases}$$

Where $m = 0, 1, 2, \ldots, M-1$, $n = 1, 2, \ldots, 2^{k-1}$, $i = n + 2^{k-1}m$, k is any +ve integer, M is the maximum degree of first kind Chebyshev wavelet. Chebyshev polynomial $T_m(\tau)$ of degree m are orthogonal with respect to the weight function $w(\tau) = \frac{1}{\sqrt{1-\tau^2}}$ on [–1,1]. The chebyshev polynomial satisfy the following recurrence formula,

$T_0(\tau) = 1$,
$T_1(\tau) = \tau$,
$T_{m+1} = 2\tau\, T_m(\tau) - T_{m-1}(\tau), \quad \forall \quad m = 1, 2, 3, \ldots$

3. Chebyshev wavelet modified OMI

In this study, we use operational matrix of integration to analysis the considered model. The Chebyshev wavelets OMI for $k = 1$ and $M = 4$ with four basis in $[0, 1)$ is given by,

$$\left.\begin{aligned} \mathcal{C}_{1,0}(\tau) &= \tfrac{2}{\sqrt{\pi}} \\ \mathcal{C}_{1,1}(\tau) &= 2\sqrt{\tfrac{2}{\pi}}(-1 + 4\tau) \\ \mathcal{C}_{1,2}(\tau) &= 2\sqrt{\tfrac{2}{\pi}}(-1 + 2(-1 + 4\tau)^2) \\ \mathcal{C}_{1,3}(\tau) &= 2\sqrt{\tfrac{2}{\pi}}(-3(-1 + 4\tau) + 4(-1 + 4\tau)^3) \end{aligned}\right\} \quad (3.1)$$

by using $t_i = \frac{i-0.5}{2^k M}$, where $i = 1, 2, \ldots, 2^{k-1}M$ as the collocation points. Collocating the base functions with above mentioned collocation points the corresponding $\mathcal{C}$ matrix can be represented as:

$$\mathcal{C} = \begin{pmatrix} 1.12837 & 1.12837 & 1.12837 & 1.12837 \\ -1.19683 & -0.398942 & 0.398942 & 1.19683 \\ 0.199471 & -1.3963 & -1.3963 & 0.199471 \\ 0.89762 & 1.09709 & -1.09709 & -0.89762 \end{pmatrix}$$

Integrate Eq. (3.1) concerning τ from 0 to τ we

get,

$$\left.\begin{aligned}
&\int_0^1 \mathcal{C}_{1,0}(\tau) = \tfrac{2\tau}{\sqrt{\pi}} \\
&\int_0^1 \mathcal{C}_{1,1}(\tau) = -2\sqrt{\tfrac{2}{\pi}}\,\tau + 4\sqrt{\tfrac{2}{\pi}}\,\tau^2 \\
&\int_0^1 \mathcal{C}_{1,2}(\tau) = 2\sqrt{\tfrac{2}{\pi}}(\tau - 8\,\tau^2 + \tfrac{32\tau^3}{3}) \\
&\int_0^1 \mathcal{C}_{1,3}(\tau) = 2\sqrt{\tfrac{2}{\pi}}\,\tau(-1 + 18\,\tau - 64\,\tau^2 + 64\,\tau^3)
\end{aligned}\right\} \tag{3.2}$$

To obtain first OMI $\mathcal{C}'$, collocate equation Eq. (3.2) with collocation points,

$$\mathcal{C}' = \begin{pmatrix} 0.0705237 & 0.211571 & 0.352618 & 0.493666 \\ -0.0872686 & -0.187004 & -0.187004 & -0.0872686 \\ 0.0540234 & -0.0374008 & -0.228561 & -0.319985 \\ -0.0109086 & 0.163629 & 0.163629 & -0.0109086 \end{pmatrix}$$

Similarly, we can obtain OMI with a different sequence.

4. Chebyshev wavelet method

The most popular numerical technique for solving ODEs, PDEs, SODEs, SPDEs, and fractional DEs is collocation. This strategy can be applied in two ways to improve the accuracy of the solutions. First, by shrinking the domain and adding additional base elements. In order to obtain the required level of precision in the result, we concurrently implemented both in the current experiment. By breaking up the provided domain into smaller segments, we can select more base elements. In the end, we combine these solutions in a straight line. We take into consideration the interval $[\frac{n-1}{2^{k-1}}, \frac{n}{2^{k-1}}]$ as follows, the expression $B_k = \cup_{n=1}^{2^{k-1}} [\frac{n-1}{2^{k-1}}, \frac{n}{2^{k-1}}]$, where $k = 1, 2, \ldots$ and $n = 1, 2, \ldots, 2^{k-1}$.
Consider the approximation as

$$z'_{i,k}(\tau) = \sum_{n=1}^{2^{k-1}} \sum_{m=0}^{M-1} q^i_{n,m}\,\phi_{n,m}(\tau), \tag{4.1}$$

where k denotes the solution's domain and i denotes the independent variables. Chebyshev wavelet unknown coefficients $Q^i_{n,m}$ and wavelet basis elements are $\phi_{n,m}(\tau)$.

$$z'_{i,k} = Q^i_{n,m}\,\Phi_{n,m}(\tau), \tag{4.2}$$

where, $Q^i_{n,m} = [q^i_{1,0},\ q^i_{1,1},\ \ldots\ q^i_{1,M-1},\ q^i_{2,0}, \ldots\ q^i_{2,M-1}, \ldots\ q^i_{2^{k-1},0}, \ldots\ q^i_{2^{k-1},M-1}]$
$\Phi_{n,m}(\tau) = [\phi_{1,0}(\tau), \ldots\ \phi_{1,M-1}(\tau),\ \phi_{2,0}(\tau), \ldots\ \phi_{2,M-1}(\tau), \ldots\ \phi_{2^{k-1},0}(\tau), \ldots\ \phi_{2^{k-1},M-1}(\tau)]^T$

Define characteristic function

$$\Delta(\tau)_{\substack{\text{specific one} \\ \text{linked portion of } B_k}} = \begin{cases} 1, if\ \tau \in specific\ one\ linked\ portion\ of\ B_k, \\ 0, if\ \tau \notin specific\ one\ linked\ portion\ of\ B_k. \end{cases}$$

The general approximation is considered as,

$$Z'_i(\tau) = \sum_{\substack{\text{vary on each} \\ \text{components of } B_k}} \Delta_k(\tau)\, z'_{i,k}(\tau), \quad \forall \tau \in B_k,\ k \in N$$

Now, let's select the collocation points as $\tau_j = \frac{i_j - 1}{2^k(2^{k-1})M}$, where $i_{j=1,\ldots,k} = 1, 2, \ldots, 2^{k-1}M$.

$$Z'_i(\tau_j) = \sum_{\substack{\text{vary on each} \\ \text{components of } B_k}} \Delta(\tau_j)\, z'_{i,k}(\tau_j) \tag{4.3}$$

The matrix representation of Eq. (4.3) is

$$Z'_i(\tau_j) = \sum \Delta_k(\tau_j)\, Q^i_{n,m}\, C_{B_k}, \tag{4.4}$$

where Section 2 defines C_{Dk}. Following Eq. (4.4) integration. We obtain,

$$Z_i(\tau_j) = Z_i(0) + \sum \Delta(\tau_j)\, Q^i_{n,m}\, C'_{B_k} \tag{4.5}$$

Replace Eqs. (4.3) and (4.5) in the model that is provided. The system of equations we derive is as follows:

$$\begin{aligned}
&Z_i(Q^1_{1,0}, \ldots, Q^1_{1,M-1}, Q^1_{2,0}, \ldots, Q^1_{2,M-1}, Q^1_{2^{k-1},0}, \ldots, \\
&Q^1_{2^{k-1},M-1}, Q^2_{1,0}, \ldots, Q^2_{1,M-1}, \ldots, Q^2_{2^{k-1},0}, \ldots, \\
&Q^2_{2^{k-1},M-1}, \ldots, Q^2_{2^{k-1},0}, \ldots, Q^2_{2^{k-1},M-1}, Q^3_{1,0}, \ldots, \\
&Q^3_{1,M-1}, \ldots, Q^3_{2^{k-1},0}, \ldots, Q^3_{2^{k-1},M-1}) = 0,
\end{aligned}$$

where, $i = 1, 2, \ldots, 3\,2^{k-1}M$.

The Newton-Raphson approach is used in the following ways to get the values of the Chebyshev wavelet coefficients $Q^1_{n,m}$,..., $Q^3_{n,m}$. Regarding $K = 1, 2, 3$. The slope intercept point is $Q^K_{(n,m),\,i+1}$ which may be written using Taylor series expansion. The $Q^K_{n,m}$ represents the initial guess of the root,

Table 3. Numerical depiction of $\mathcal{X}$ with various methods

τ	NDSolve	RK4	CWCM	AE of RK4 with NDSolve	AE of CWCM with NDSolve
0	476.0000	476.0000	476.0000	0	0
0.1	476.0013	476.0013	476.0013	6.182×10^{-3}	3.618×10^{-7}
0.2	476.0026	476.0026	476.0026	2.112×10^{-3}	1.211×10^{-6}
0.3	476.0039	476.0039	476.0039	1.248×10^{-3}	2.124×10^{-6}
0.4	476.0051	476.0051	476.0051	6.846×10^{-3}	2.684×10^{-6}
0.5	476.0064	476.0064	476.0064	7.407×10^{-3}	2.874×10^{-6}
0.6	476.0076	476.0076	476.0076	5.554×10^{-3}	3.555×10^{-6}
0.7	476.0087	476.0087	476.0087	4.172×10^{-3}	4.417×10^{-6}
0.8	476.0099	476.0098	476.0098	5.132×10^{-3}	5.051×10^{-6}
0.9	476.0110	476.0110	476.0110	5.575×10^{-3}	5.157×10^{-6}
1	476.0120	476.0120	476.0120	5.583×10^{-3}	5.558×10^{-6}

$$Z_{1,i+1} = Z_{1,i} + (Q^K_{(1,0),i+1} - Q^K_{(1,0),i})\frac{\partial Z_{1,i}}{\partial Q^K_{(1,0)}} + (Q^K_{(2,0),i+1} - Q^K_{(2,0),i})\frac{\partial Z_{1,i}}{\partial Q^K_{(2,0)}} +, \ldots, + (Q^K_{(2^{k-1},M-1),i+1} - Q^K_{(2^{k-1},M-1),i})\frac{\partial Z_{1,i}}{\partial Q^K_{(2^{k-1},M-1)}},$$

Applying the same method of Taylor series expansion for $Z_2, \ldots, Z_{3\,2^{k-1}M}$ and expanding it to $3\,2^{k-1}M$ equations, we obtain

$$\frac{\partial Z_{k,i}}{\partial Q^K_{(1,0)}} Q^K_{1,i+1} + \frac{\partial Z_{k,i}}{\partial Q^K_{(2,0)}} Q^K_{2,i+1} +, \ldots, + \frac{\partial Z_{k,i}}{\partial Q^K_{(2^{k-1},M-1)}} Q^K_{m,i+1} = -Z_{k,i} + Q^K_{1,i}\frac{\partial Z_{k,i}}{\partial Q^K_{(1,0)}} + Q^K_{2,i}\frac{\partial Z_{k,i}}{\partial Q^K_{(2,0)}} +, \ldots, + Q^K_{m,i}\frac{\partial Z_{k,i}}{\partial Q^K_{(2^{k-1},M-1)}}, \quad (4.6)$$

The function at the current value (i) or at the next value $(i+1)$ is indicated by the second subscript, whereas the equations are indicated by the first subscript k. For Section 4, the matrix notation is as follows:

$$[P][Q^K_{i+1}] = -[Z] + [P][Q^K_i]. \quad (4.7)$$

The Jacobian matrix made up of partial derivatives is used to express the partial derivatives assessed at i:

$$[P] = \begin{bmatrix} \frac{\partial Z_{1,i}}{\partial Q^K_{(1,0)}} & \frac{\partial Z_{1,i}}{\partial Q^K_{(2,0)}} & \cdots & \frac{\partial Z_{1,i}}{\partial Q^K_{(2^{k-1},M-1)}} \\ \frac{\partial Z_{2,i}}{\partial Q^K_{(1,0)}} & \frac{\partial Z_{2,i}}{\partial Q^K_{(2,0)}} & \cdots & \frac{\partial Z_{2,i}}{\partial Q^K_{(2^{k-1},M-1)}} \\ \vdots & & \cdots & \vdots \\ \frac{\partial Z_{3\,2^{k-1}M,i}}{\partial Q^K_{(1,0)}} & \frac{\partial Z_{3\,2^{k-1}M,i}}{\partial Q^K_{(2,0)}} & \cdots & \frac{\partial Z_{3\,2^{k-1}M,i}}{\partial Q^K_{(2^{k-1},M-1)}} \end{bmatrix}$$

The vector form expression for the start and final values is as follows:

$$[Q^K_i]^T = [Q^K_{(1,0),i} Q^K_{(2,0),i} \cdots Q^K_{(2^{k-1},M-1),i}], \quad [Q^K_{i+1}]^T = [Q^K_{(1,0),i+1} Q^K_{(2,0),i+1} \cdots Q^K_{(2^{k-1},M-1),i+1}], \quad \text{and} \quad [Z]^T = [Z_{1,i} Z_{2,i} \cdots Z_{3\,2^{k-1}M,i}]$$

Eq. (4.7) is multiplied with $[P]^{-1}$

$$[Q^K_{i+1}] = [Q^K_i] - [Q]^{-1}[Z]. \quad (4.8)$$

Using Eq. (4.8), we get the Chebyshev wavelet coefficients $Q^K_{n,m}$. By replacing $Q^K_{n,m}$, we obtain the desired solution of Eq. (4.5).

5. Numerical results

The mathematical model Eq. (1.1) presents the emanations of CO_2 from energy sector which is solved using the operational matrix presented in section 3 and Chebyshev wavelet method in section 4. We applied the Chebyshev wavelet collocation method to transform the set of nonlinear differential equations into a set of algebraic equations. Later, using the Newton-Raphson method, the set of nonlinear algebraic equations is solved and the Chebyshev wavelet coefficients are obtained. By substituting these coefficient values, wavelet-based numerical solutions of $\mathcal{X}(\tau)$, $\mathcal{Y}(\tau)$, and $\mathcal{F}(\tau)$ are obtained for the model. Tables 3 to 5 display the CWCM solutions acquired for the $\alpha = 1$ (integer order), demonstrating that the suggested solutions are quite similar to the NDSolve results in contrast to the RK4 technique. Since there isn't an exact solution, the numerical approximations produced by the developed technique (CWCM) and RK4 methods are compared with the NDSolve solution. The absolute error (AE) of the developed approach with the NDSolve solution are also tabulated in the Tables 3 to 5. The pictorial depition of solutions of NDSolve, RK4, and CWCM are shown in Figs. 1, 3 and 5. Error analysis of $\mathcal{X}(\tau)$, $\mathcal{Y}(\tau)$ and $\mathcal{F}(\tau)$ is represented in Figs. 2, 4 and 6 which shows that the AE of CWCM is approaching to Zero when compared to RK4 method. It is clear that compared to other methods currently in use, the errors obtained

Table 4. Numerical depiction of $\mathcal{Y}$ with various methods.

τ	NDSolve	RK4	CWCM	AE of RK4 with NDSolve	AE of CWCM with NDSolve
0	660.0000	660.0000	660.0000	0	0
0.1	660.0005	660.0005	660.0005	1.318×10^{-4}	3.148×10^{-8}
0.2	660.0010	660.0010	660.0010	4.389×10^{-4}	8.439×10^{-8}
0.3	660.0015	660.0015	660.0015	7.670×10^{-4}	6.540×10^{-8}
0.4	660.0021	660.0021	660.0015	9.650×10^{-4}	5.965×10^{-8}
0.5	660.0026	660.0026	660.0026	1.025×10^{-3}	2.051×10^{-7}
0.6	660.0031	660.0031	660.0031	1.259×10^{-3}	9.125×10^{-7}
0.7	660.0036	660.0036	660.0036	1.557×10^{-3}	3.615×10^{-7}
0.8	660.0042	660.0042	660.0042	1.777×10^{-3}	1.762×10^{-7}
0.9	660.0047	660.0047	660.0047	1.818×10^{-3}	1.777×10^{-7}
1	660.0052	660.0052	660.0052	1.973×10^{-3}	1.880×10^{-7}

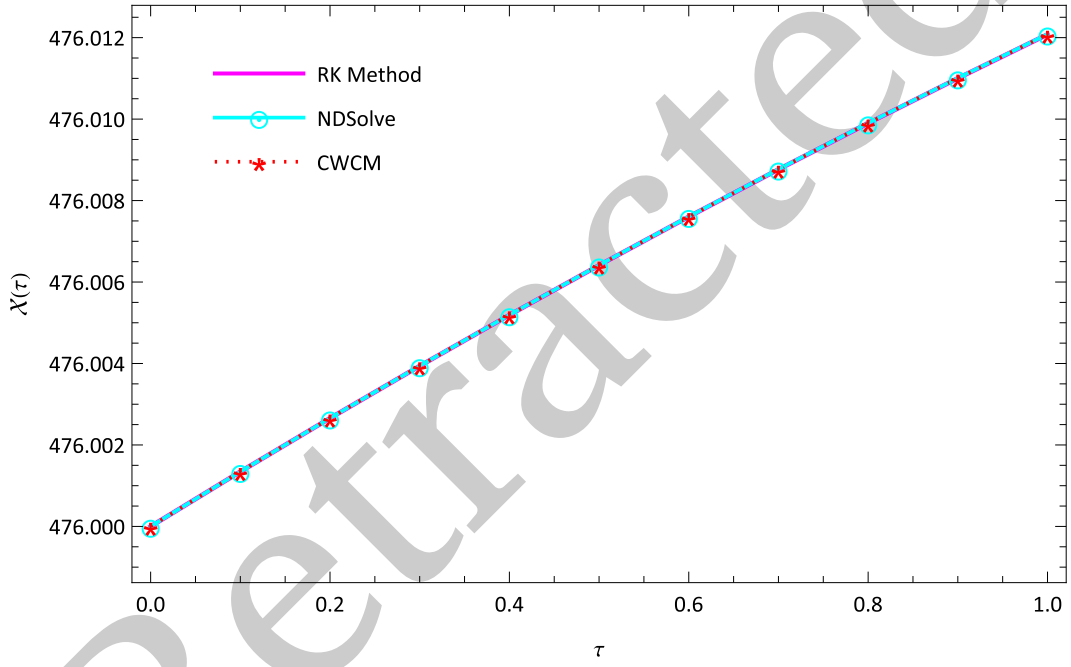

Fig. 1. Pictorial depiction of $\mathcal{X}(\tau)$ solution with different methods.

with the predicted CWCM are smaller. The model's numerical approximation for various β values is calculated and presented in Tables 6 to 8. Figs. 7 to 9 show the solution graphically for $\beta = 0.3$, 0.5, and 0.8, respectively. Thus, we may infer from the graphical data that the model's realistic results are largely dependent on the sequence of fractional derivatives. Furthermore, we deduce that the proposed model under Caputo fractional order derivative provides more flexible and prosperous results than the energy sector model's equivalent integer order of emanation of CO_2.

Variation of depletion rate coefficient of human population due to CO_2 (γ): The graphic representation of the variation of $\mathcal{X}(\tau)$, $\mathcal{Y}(\tau)$, $\mathcal{F}(\tau)$ that affects the concentration of CO_2 in the atmosphere, concentration of CO_2 due to human population, concentration of CO_2 due to forest biomass are shown in Fig. 10. As the depletion rate coefficient of human population due to CO_2 (γ) rises, the concentration of CO_2 in the atmosphere $\mathcal{X}(\tau)$, concentration of CO_2 due to human population $\mathcal{Y}(\tau)$ decreases, whereas concentration of CO_2 due to forest biomass $\mathcal{F}(\tau)$ increases.

Variation of intrinsic growth rate of forest biomass (σ): The graphic representation of the variation of $\mathcal{X}(\tau)$, $\mathcal{Y}(\tau)$, $\mathcal{F}(\tau)$ that affects the concentration of CO_2 in the atmosphere, concentration of CO_2 due to human population, concentration of CO_2 due to forest biomass are shown in Fig. 11. As the intrinsic growth rate of forest biomass (σ) rises, the concentration of CO_2 in the atmosphere $\mathcal{X}(\tau)$ decreases, whereas concentration of CO_2 due to human population $\mathcal{Y}(\tau)$, and concentration of CO_2 due to forest biomass $\mathcal{F}(\tau)$ increases.

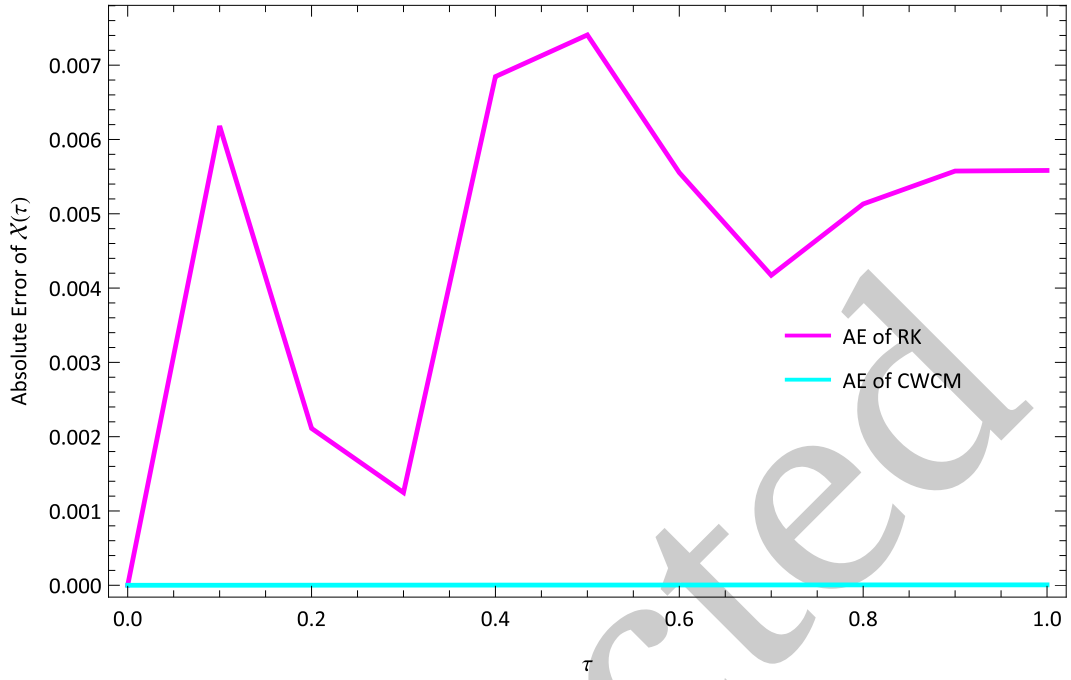

Fig. 2. Absolute Error analysis of $\mathcal{X}(\tau)$.

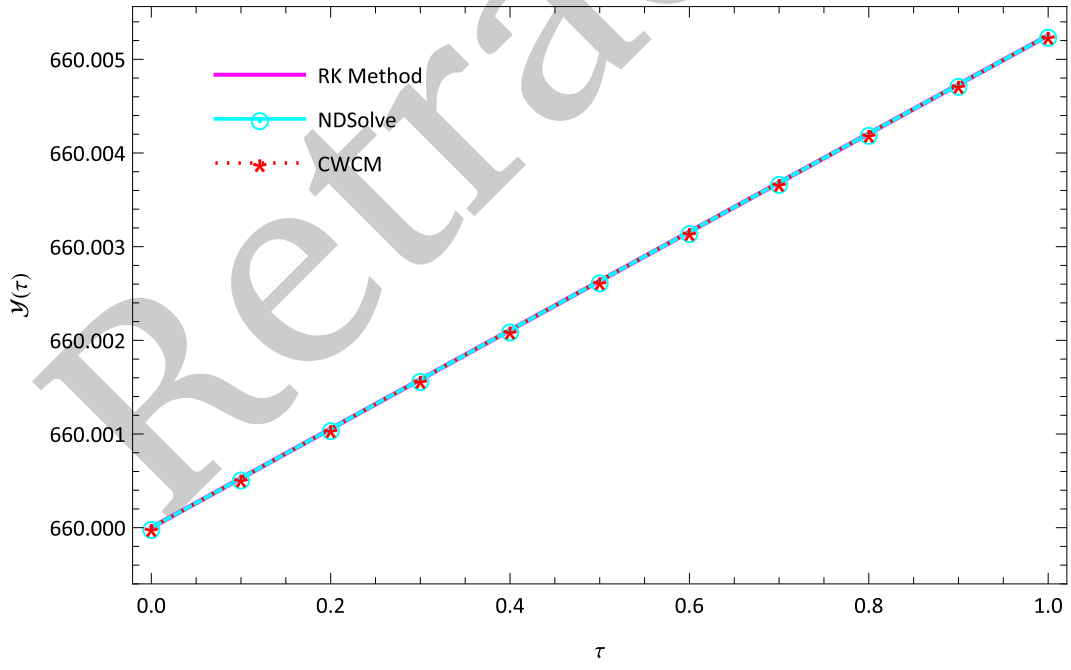

Fig. 3. Pictorial depiction of $\mathcal{Y}(\tau)$ solution with different methods.

Variation of growth rate of atmospheric CO_2 due to natural causes (λ): The graphic representation of the variation of $\mathcal{X}(\tau)$, $\mathcal{Y}(\tau)$, $\mathcal{F}(\tau)$ that affects the concentration of CO_2 in the atmosphere, concentration of $C0_2$ due to human population, concentration of CO_2 due to forest biomass are shown in Fig. 12. As the growth rate of atmospheric CO_2 due to natural causes (λ) rises, the concentration of CO_2 in the atmosphere $\mathcal{X}(\tau)$, and concentration of CO_2 due to forest biomass $\mathcal{F}(\tau)$ increases, whereas concentration of CO_2 due to human population $\mathcal{Y}(\tau)$ decreases.

Variation of intrinsic growth rate of human population (ϕ): The graphic representation of the variation of $\mathcal{X}(\tau)$, $\mathcal{Y}(\tau)$, $\mathcal{F}(\tau)$ that affects the concentration of CO_2 in the atmosphere, concentration of

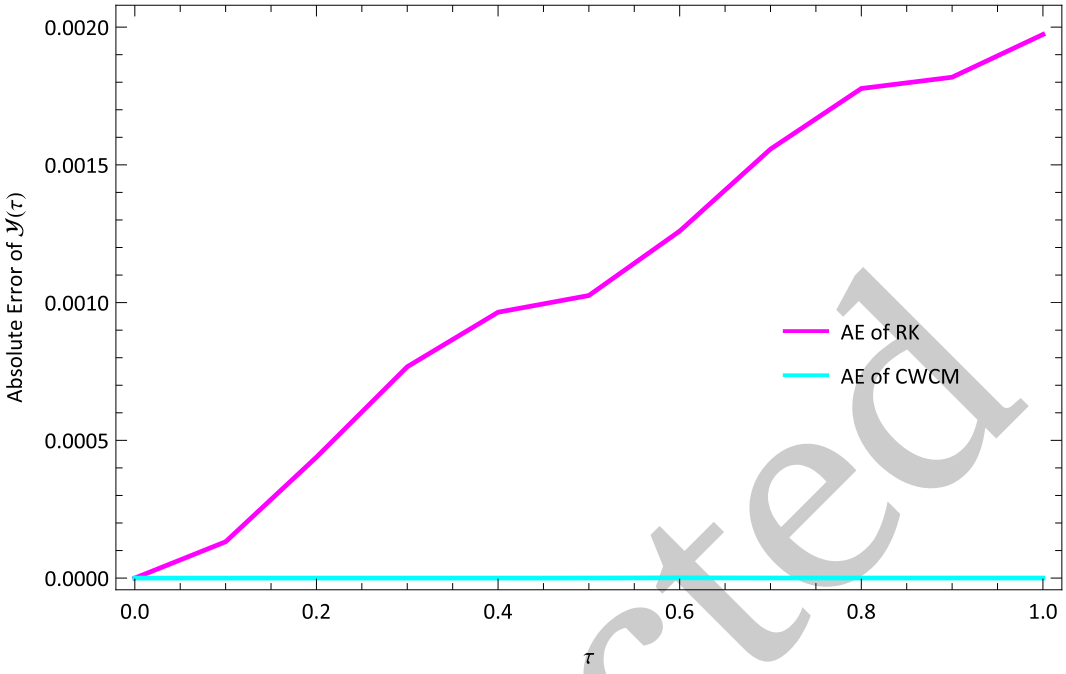

Fig. 4. Absolute error analysis of $\mathcal{Y}(\tau)$.

Table 5. Numerical depiction of $\mathcal{F}$ with various methods.

τ	NDSolve	RK4	CWCM	AE of RK4 with NDSolve	AE of CWCM with NDSolve
0	684.0000	684.0000	684.0000	0	0
0.1	684.0051	684.0051	684.0051	2.505×10^{-3}	2.506×10^{-7}
0.2	684.0103	684.0103	684.0103	8.447×10^{-3}	7.128×10^{-7}
0.3	684.0154	684.0154	684.0154	1.485×10^{-3}	5.264×10^{-6}
0.4	684.0204	684.0204	684.0204	1.881×10^{-3}	3.884×10^{-6}
0.5	684.0254	684.0254	684.0254	2.020×10^{-3}	8.920×10^{-6}
0.6	684.0304	684.0304	684.0304	2.509×10^{-3}	9.250×10^{-6}
0.7	684.0353	684.0353	684.0353	3.131×10^{-3}	1.325×10^{-6}
0.8	684.0402	684.0402	684.0402	3.604×10^{-3}	6.047×10^{-6}
0.9	684.0450	684.0450	684.0450	3.724×10^{-3}	4.723×10^{-6}
1	684.0499	684.0499	684.0499	4.088×10^{-3}	8.088×10^{-6}

Table 6. Numerical depiction of $\mathcal{X}$ for various values of β.

	CWCM		
τ	$\beta = 0.8$	$\beta = 0.5$	$\beta = 0.3$
0	476.0000	476.0000	476.0000
0.1	476.0079	476.0044	476.0028
0.2	476.0089	476.0061	476.0045
0.3	476.0095	476.0074	476.0059
0.4	476.0100	476.0084	476.0071
0.5	476.0107	476.0093	476.0082
0.6	476.0125	476.0104	476.0093
0.7	476.0165	476.0120	476.0104
0.8	476.0238	476.0142	476.0116
0.9	476.0352	476.0174	476.0131

Table 7. Numerical depiction of $\mathcal{Y}$ for various values of β.

	CWCM		
τ	$\beta = 0.8$	$\beta = 0.5$	$\beta = 0.3$
0	660.0000	660.0000	660.0000
0.1	660.0035	660.0018	660.0011
0.2	660.0041	660.0026	660.0018
0.3	660.0044	660.0032	660.0024
0.4	660.0047	660.0037	660.0030
0.5	660.0050	660.0041	660.0035
0.6	660.0059	660.0047	660.0040
0.7	660.0077	660.0054	660.0045
0.8	660.0109	660.0063	660.0051
0.9	660.0159	660.0077	660.0058

CO_2 due to human population, concentration of CO_2 due to forest biomass are shown in Fig. 13. As the intrinsic growth rate of human population (ϕ) rises, the concentration of CO_2 in the atmosphere $\mathcal{X}(\tau)$, and concentration of CO_2 due to human population $\mathcal{Y}(\tau)$ increases, whereas the concentration of CO_2 due to forest biomass $\mathcal{F}(\tau)$ decreases.

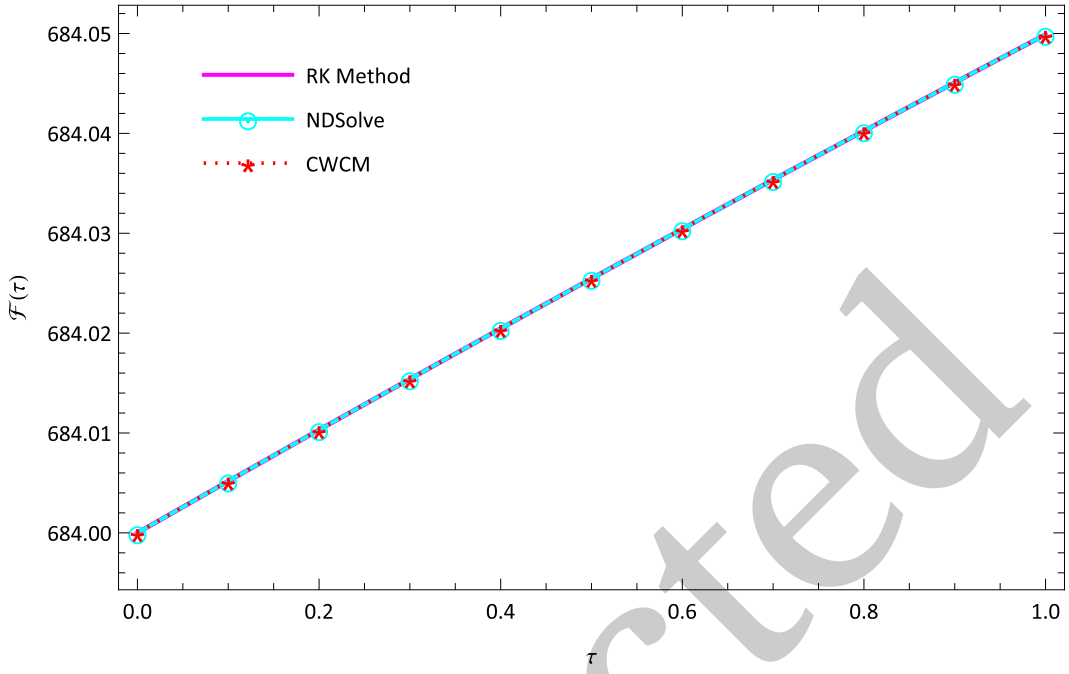

Fig. 5. Pictorial depiction of $\mathcal{F}(\tau)$ solution with different methods.

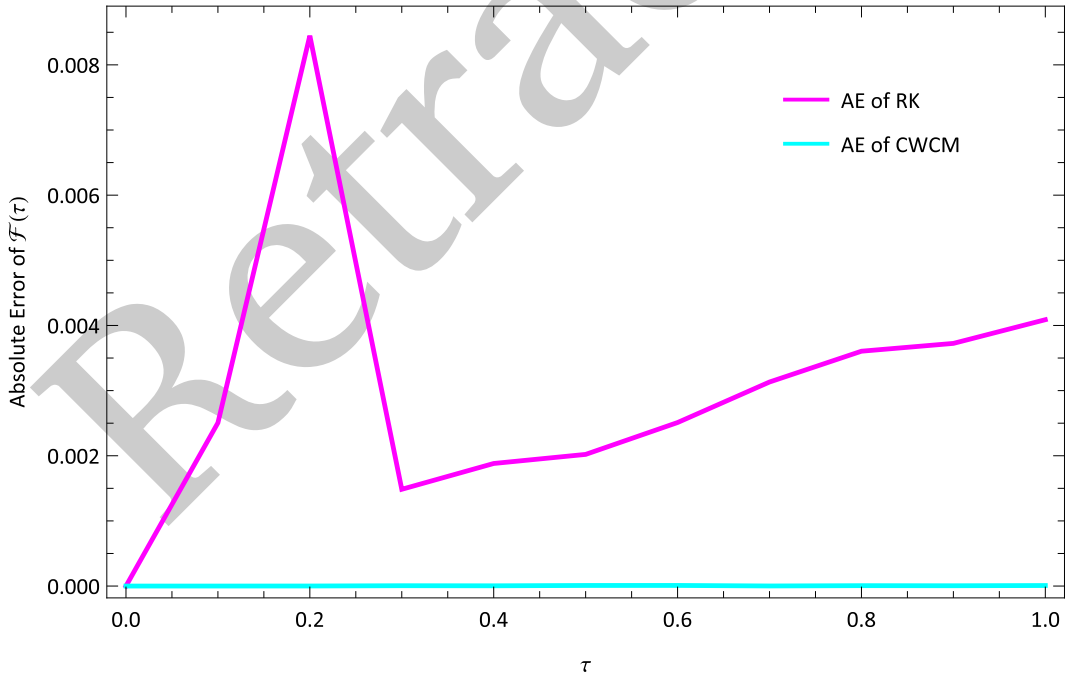

Fig. 6. Absolute error analysis of $\mathcal{F}(\tau)$.

6. Conclusion

In this study, we have studied the fractional order model of the Emanation of CO_2 from the Energy Sector with the help of the CWCM. The model is solved numerically and the effect of variation of parameters is studied using the collocation approach, operational matrix constructed from the Chebyshev wavelets, and Chebyshev wavelet method. Techniques like RK4 and ND Solver have been used to compare the solutions derived from the developed method. The outcomes of this approach are well-aligned with the ND Solver in Mathematica. The findings show that the proposed approach outperforms the existing numerical tech-

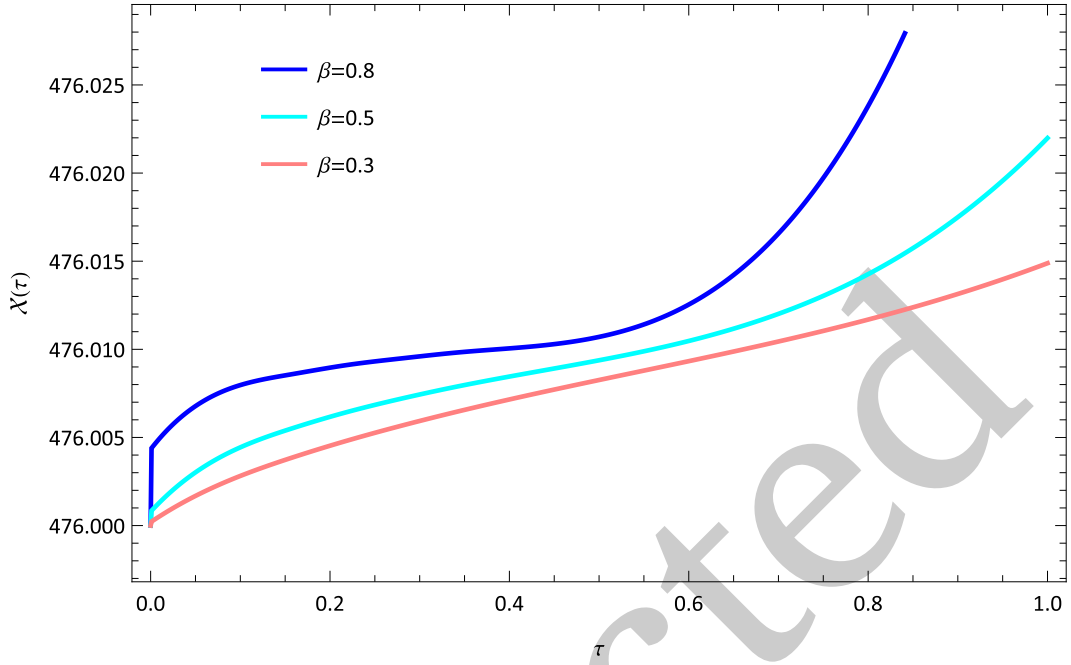

Fig. 7. Pictorial depiction of $\mathcal{X}(\tau)$ for various values of β.

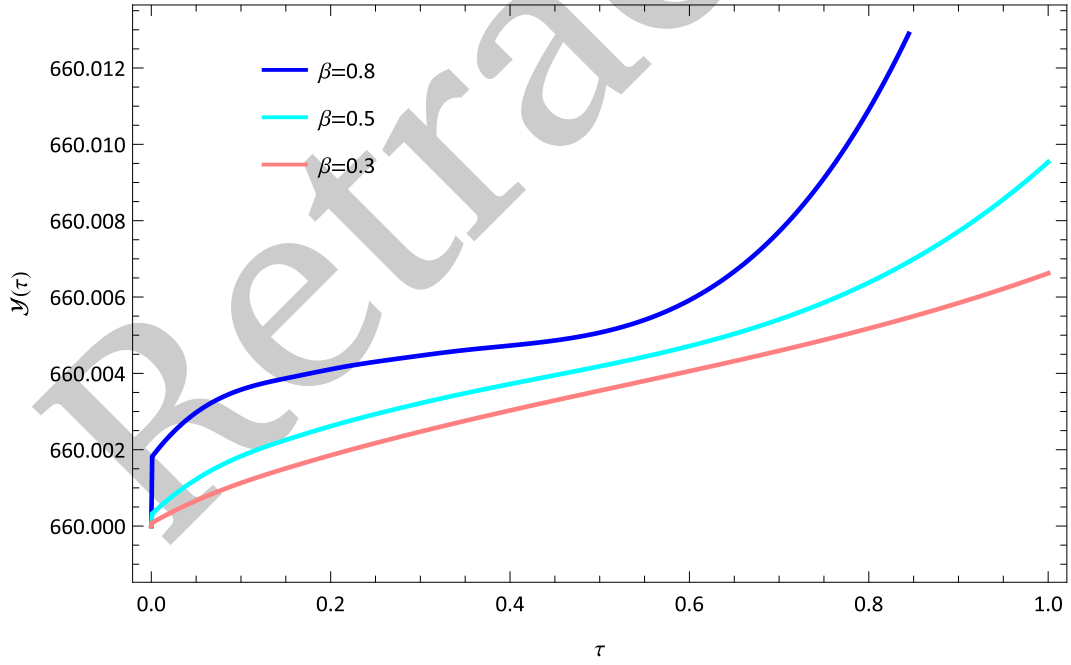

Fig. 8. Pictorial depiction of $\mathcal{Y}(\tau)$ for various values of β.

niques in terms of precision. The notion that only a small number of Chebyshev wavelets are needed to achieve appropriate results is further supported by numerical examples. The technique was easy to implement and produced a really good finish. It confirmed our belief that the method is a practical way to deal with extremely nonlinear FDs. The method under discussion is straightforward, easy to use, and requires less computing power. Different values of M and k can be used to calculate CWCM solutions. Additionally, we can increase the precision of the result by increasing the values of M and k. We therefore came to the conclusion that the present approach is a well-known instrument for obtaining the numerical approximation of the mathematical models in the form of nonlinear FD, in contrast to RK4

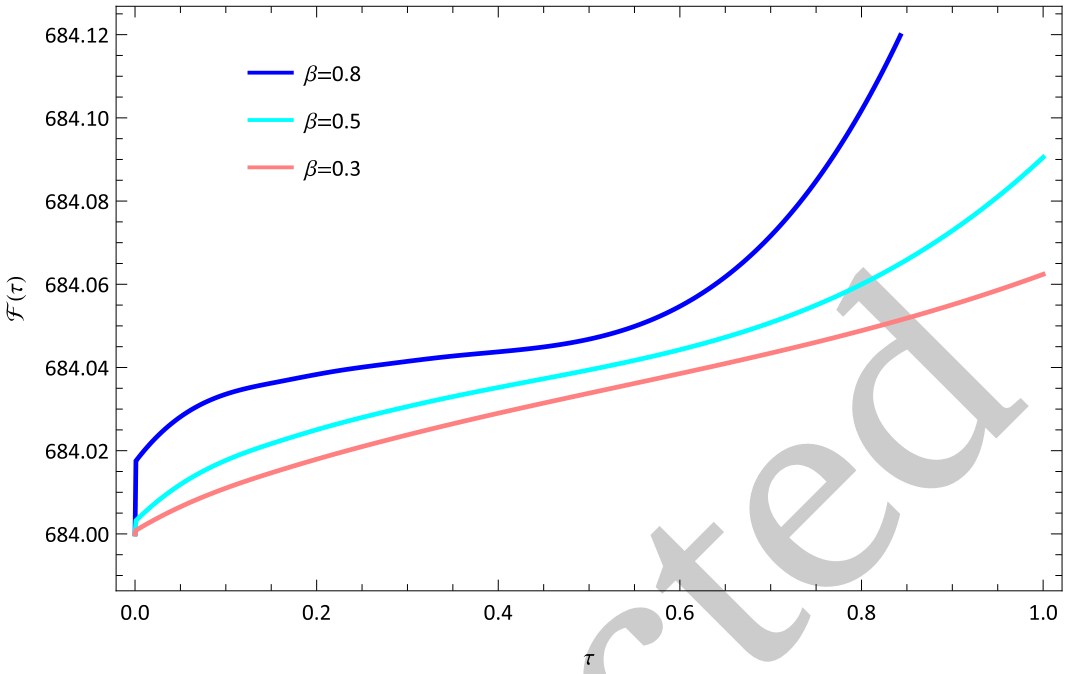

Fig. 9. Pictorial depiction of $\mathcal{F}(\tau)$ for various values of β.

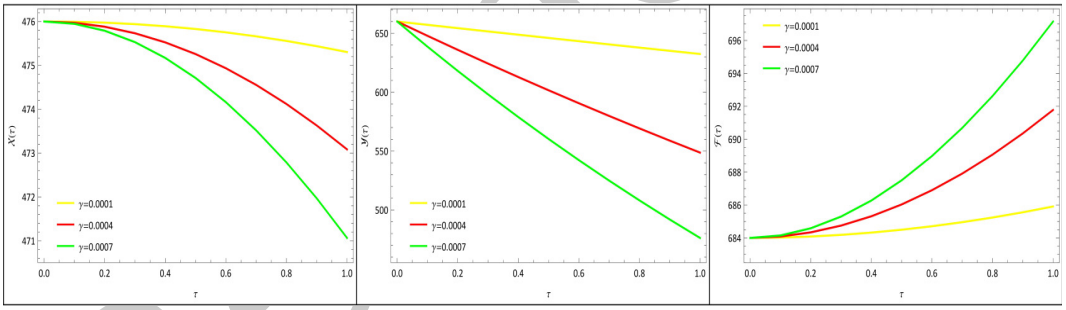

Fig. 10. Pictorial depiction of variation of γ.

and ND Solver. This approach is also applicable to other higher order mathematical models with slight modification.

Acknowledgements

The authors express their affection for the DST-SERB, Govt. of India. New Delhi for the financial

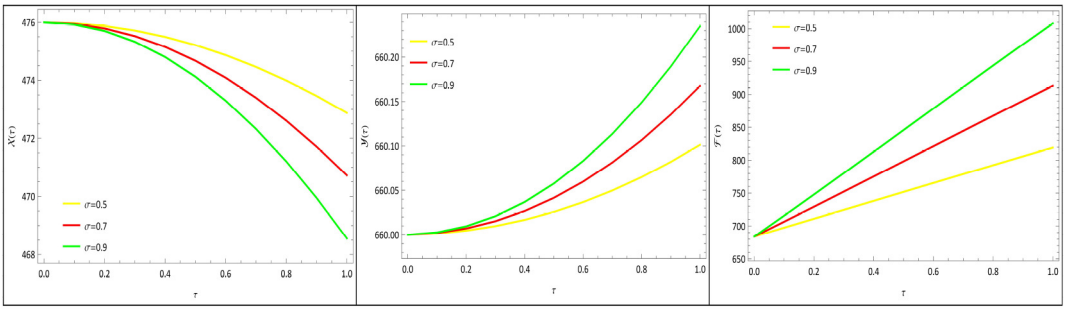

Fig. 11. Pictorial depiction of variation of σ.

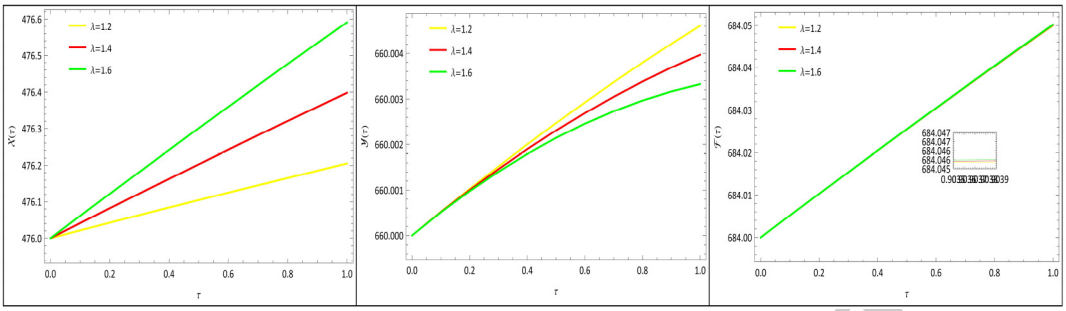

Fig. 12. Pictorial depiction of variation of λ.

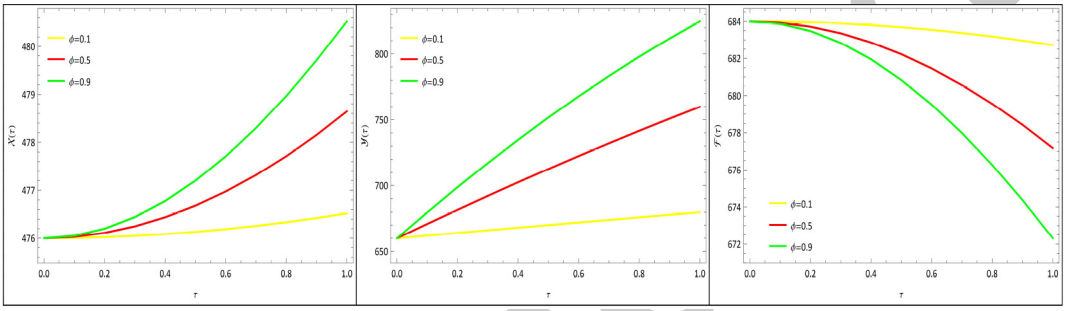

Fig. 13. Pictorial depiction of variation of ϕ.

Table 8. Numerical depiction of $\mathcal{F}$ for various values of β

	CWCM		
τ	$\beta = 0.8$	$\beta = 0.5$	$\beta = 0.3$
0	684.0000	684.0000	684.0000
0.1	684.0335	684.0176	684.0110
0.2	684.0383	684.0250	684.0179
0.3	684.0414	684.0305	684.0237
0.4	684.0437	684.0351	684.0290
0.5	684.0468	684.0394	684.0338
0.6	684.0547	684.0442	684.0385
0.7	684.0716	684.0507	684.0434
0.8	684.1018	684.0599	684.0488
0.9	684.1494	684.0728	684.0550

support under Empowerment and Equity Opportunities for Excellence in Science for 2023-2026. F.No.EEQ/2022/620 Dated:07/02/2023.

Declarations

- Conflict of interest: Authors state they have no Conflict of interest.
- Ethics approval and consent to participate: Not Applicable.
- Funding: The author states that no funding is involved.
- Availability of data and materials: The data supporting this study's findings are available within the article.
- Author contribution: All authors contributed equally and approved the final manuscript.

References

1. Y. Tian, K. Sun, L. Chen, and A. Kasperski, "Studies on the dynamics of a continuous bioprocess with impulsive state feedback control," *Chemical Engineering Journal*, vol. 157 no. 2-3, pp. 558–567, 2010.
2. A. A. Kilbas, H. M. Srivastava, and J. J. Trujillo, "Theory and applications of fractional differential equations" (Vol. 204). elsevier, 2006.
3. I. Podlubny, "Fractional differential equations, mathematics in science and engineering" 1999.
4. Y. A. Rossikhin and M. V. Shitikova, "Applications of fractional calculus to dynamic problems of linear and nonlinear hereditary mechanics of solids", 1997.
5. K. Shah, F. Jarad, and T. Abdeljawad, "On a nonlinear fractional order model of dengue fever disease under Caputo-Fabrizio derivative," *Alexandria Engineering Journal*, vol. 59, no. 4, pp. 2305–2313, 2020.
6. A. Atangana and S. Qureshi, "Modeling attractors of chaotic dynamical systems with fractal-fractional operators" *Chaos, Solitons & Fractals*, vol. 123, pp. 320–337, 2019.
7. S. Araz, ?, "Numerical analysis of a new volterra integro-differential equation involving fractal-fractional operators," *Chaos, Solitons & Fractals*, vol. 130, Art. no. 109396, 2020.

8. P. Priya and A. Sabarmathi, "Caputo fractal fractional order derivative of soil pollution model due to industrial and agro-chemical," *International Journal of Applied and Computational Mathematics*, vol. 8, no. 5, Art. no. 250, 2022.
9. Z. Li, Z. Liu, and M. A. Khan, "Fractional investigation of bank data with fractal-fractional Caputo derivative," *Chaos, Solitons & Fractals*, vol. 131, Art. no. 109528, 2020.
10. Statistical Review of World Energy 2019 LXVIIIEdition, London:BP https://www.bp.com/content/dam/bp/business-sites/en/global/corporate/pdfs/energy-economics/statistical-review/bp-stats-review-2019-full-report.pdf.
11. Inventory of U. S. Greenhouse Gas Emissions and Sinks: 1990-2017, https://www.epa.gov/ghgemissions/inventory-us-greenhousegas-emissions-and-sinks-1990-2017.
12. G. Zabel and E. Economics, "Peak people: the interrelationship between population growth and energy resources," *Energy Bulletin*, vol. 20, pp. 1–59, 2009.
13. M. E. Javanmard, Y. Tang, Z. Wang, and P. Tontiwachwuthikul, "Forecast energy demand, CO2 emissions and energy resource impacts for the transportation sector," *Applied Energy*, vol. 338, Art. no. 120830, 2023.
14. Z. Weng, Y. Song, H. Ma, Z. Ma, and T. Liu, "Forecasting energy demand, structure, and CO2 emission: a case study of Beijing, China," *Environment, Development and Sustainability*, vol. 25, no. 9, pp. 10369–10391, 2023.
15. M. A. L. Caetano, D. F. M. Gherardi, and T. Yoneyama, "An optimized policy for the reduction of CO2 emission in the Brazilian Legal Amazon," *Ecological modelling*, vol. 222, no. 15, pp. 2835–2840, 2011.
16. A. K. Misra and M. Verma, "A mathematical model to study the dynamics of carbon dioxide gas in the atmosphere," *Applied Mathematics and Computation*, vol. 219 no. 16, pp. 8595–8609, 2013.
17. U. Lepik, "Numerical solution of differential equations using Haar wavelets," *Mathematics and Computers In Simulation*, vol. 68, no. 2, pp. 127–143, 2005.
18. J. S. Guf and W. S. Jiang, "The Haar wavelets operational matrix of integration," *International Journal of Systems Science*, vol. 27, no. 7, pp. 623–628, 1996.
19. S. Kumbinarasaiah and R. Yeshwanth, "A study on Chlamydia transmission in United States through the Haar wavelet technique," *Results in Control and Optimization*, Art. no. 100396, 2024.
20. A. Darweesh, K. Al-Khaled, and O. A. Al-Yaqeen, "Haar Wavelets Method for Solving Class of Coupled Systems of Linear Fractional Fredholm Integro-Differential Equations". Heliyon.
21. S. Kumbinarasaiah and R. Yeshwanth, "Investigation of the wavelet method impact on the mathematical model of global warming effects on marine ecosystems," *Journal of Applied Mathematics and Computing*, pp. 1–27, 2024.
22. F. Li, H. M. Baskonus, S. Kumbinarasaiah, G. Manohara, W. Gao, and E. Ilhan, "An efficient numerical scheme for biological models in the frame of Bernoulli wavelets," *Comput Model Eng Sci*, vol. 137, no. 3, 2023.
23. S. C. Shiralashetti and S. Kumbinarasaiah, "Laguerre wavelets exact parseval frame-based numerical method for the solution of system of differential equations," *International Journal of Applied and Computational Mathematics*, vol. 6, pp. 1–16, 2020.
24. S. Kumbinarasaiah and M. P. Preetham, "Applications of the Bernoulli wavelet collocation method in the analysis of MHD boundary layer flow of a viscous fluid," *Journal of Umm Al-Qura University for Applied Sciences*, vol. 9, no. 1, pp. 1–14, 2023.
25. M. Mulimani and S. Kumbinarasaiah, "Numerical solution for a fractional operator-based mathematical model of a brain tumour," *The Journal of Analysis*, pp. 1–31, 2024.
26. M. Vivek Kumar and S. N. Mishra, "Solution of linear and nonlinear singular value problems using operational matrix of integration of Taylor wavelets" *Journal of Taibah University for Science*, vol. 17, no. 1, Art. no. 2241716, 2023.
27. S. Kumbinarasaiah and R. Yeshwanth,, "A numerical study of the evolution of smoking habit model through Haar wavelet technique," *International Journal of Dynamics and Control*, pp. 1–19, 2024.
28. R. Yeshwanth and S. Kumbinarasaiah, "Numerical analysis of Marriage-Divorce model using new modified Hermite wavelet collocation technique," 11 August 2024, PREPRINT (Version 1) available at Research Square https://doi.org/10.21203/rs.3.rs-4747668/v1.
29. K. Srinivasa and H. Rezazadeh, "Numerical solution for the fractional-order one-dimensional telegraph equation via wavelet technique," *International Journal of Nonlinear Sciences and Numerical Simulation*, vol. 22, no. 6, pp. 767–780, 2021.
30. S. C. Shiralashetti and A. B. Deshi, "The numerical solution of singular initial value problems using Chebyshev wavelet collocation method," *Ain Shams Engineering Journal*, vol. 9, no. 4, pp. 1451–1456.